Image-based analysis of the internal microstructure of bone replacement scaffolds fabricated by 3D printing

Stephan H. Irsen*[1], Barbara Leukers[1], Björn Bruckschen[1], Carsten Tille[1], Hermann Seitz[1],

Felix Beckmann[2], and Bert Müller[3]

[1]caesar Research Center, Ludwig-Erhard-Allee 2, 53175 Bonn

[2]GKSS Research Center, Max-Planck-Str. 1, 21502 Geesthacht, Germany

[3]Computer Vision Laboratory, ETH Zurich, Sternwartstrasse 7, 8092 Zürich, Switzerland

ABSTRACT

Rapid Prototyping and especially the 3D printing, allows generating complex porous ceramic scaffolds directly from powders. Furthermore, these technologies allow manufacturing patient-specific implants of centimeter size with an internal pore network to mimic bony structures including vascularization. Besides the biocompatibility properties of the base material, a high degree of open, interconnected porosity is crucial for the success of the synthetic bone graft. Pores with diameters between 100 and 500 μm are the prerequisite for vascularization to supply the cells with nutrients and oxygen, because simple diffusion transport is ineffective. The quantification of porosity on the macro-, micro-, and nano-meter scale using well-established techniques such as Hg-porosimetry and electron microscopy is restricted. Alternatively, we have applied synchrotron-radiation-based micro computed tomography (SRμCT) to determine the porosity with high precision and to validate the macroscopic internal structure of the scaffold. We report on the difficulties in intensity-based segmentation for nanoporous materials but we also elucidate the power of SRμCT in the quantitative analysis of the pores at the different length scales.

Keywords: Rapid Prototyping, 3D printing, μ-computed tomography, bone graft

1. INTRODUCTION

Synthetic Bone Replacement

The treatment of congenitally, traumatically or surgically caused bone defects is a major problem in reconstructive surgery [1]. Today especially autogenous materials are used to fill larger cavities. Other bone grafts are based on xenogenous or synthetic materials. While these implant materials are still problematic concerning osteointegration and mechanical stability, the autologous implants need to be extracted and it is often difficult to find the suitable extraction site. Therefore, an urgent need exists for synthetic bone replacement with reasonable in-growth behavior and enhanced mechanical stability.

For the defect reconstruction, the scaffold has to be adapted to the patient's cavity to guide vascularization and osteointegration.

Rapid Prototyping

Rapid Prototyping (RP) is the term for a growing class of generative fabrication techniques, mainly used in the automotive and consumer goods industry [2]. Recently RP-technologies have been used for medical purposes including the fabrication of anatomical models in oral and maxillofacial surgery. Such models play a crucial role in preoperative planning [3].

In RP-processes, models are built layer-by-layer based on a 3-dimensional (3D) dataset, as described in figure 1. Prior to fabrication the 3D dataset is sliced into a stack of layers to be processed by the RP machine. Depending on the used RP process, various polymers, metals, and ceramics or even wax can be used.
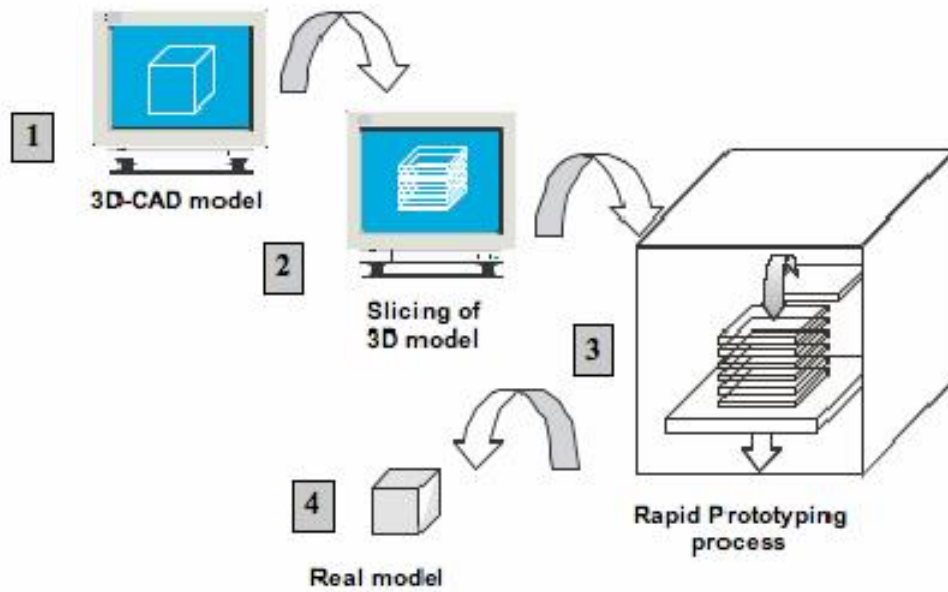
Fig. 1 General workflow of Rapid Prototyping.

For the fabrication of ceramic parts, including bone grafts, 3D printing (3DP) is well suited. In 3DP, powder or granular material is selectively glued using ink jet printer technology. The process starts with a 3D dataset that is sliced by a computer in order to generate the print matrix of each layer. The so called recoating mechanism of the 3D printer carries an amount of ceramic powder from the powder reservoir to the building box, thereby creating a thin layer of powder onto the top of the building box. Liquid binder is printed on the layer of powder according to the current cross-section of the part using a micro-dispensing valve. The ceramic powder is bonded in these selected regions. When the layer is completed, the building box piston moves down by the thickness of a layer and a new layer of powder is deposited on the first one. These process steps are repeated until the whole part is formed within the powder bed. The surrounding powder material supports the part during the building process. Thus, there is no need for support structures for features such as large overhangs. After completion, the part is removed from the building box and can cleaned using an air blower.
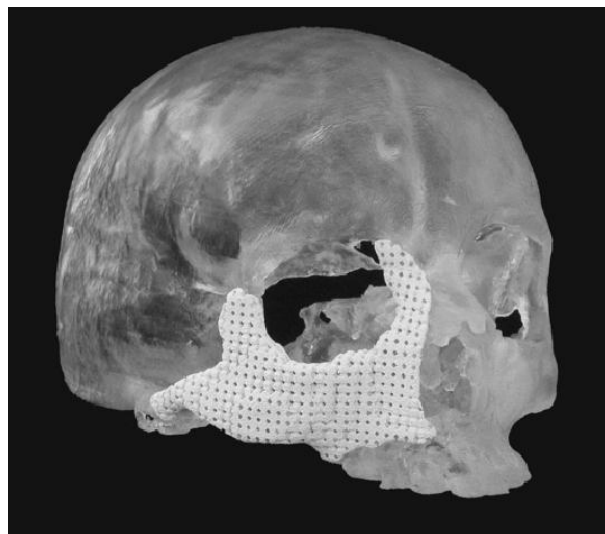

Fig. 2 Concept model of a 3D printed bone replacement implant for a tumor resection in the maxilla. For better illustration of the patient individual design, the implant is placed in an anatomical skull model. The implant features an internal channel structure with a channel-to-channel distance of about 5 mm.

Overall, RP-technology allows the fabrication of physical models with nearly no limitation in outer shape. Even more important, a great variety of internal structures can be realized. The data for the clinical morphology can be derived from computed tomography (CT) data, while the internal structure has to guarantee the cell in-growth and nutrition supply.

Requirements for scaffold design

Biocompatibility and especially mechanical stability and porosity are crucial for the quality of synthetic bone grafts. Hydroxyapatite (HA) is well established as biomaterial for this purpose [4].

To optimize mechanical stability of 3DP scaffolds, the so-called green bodies undergo post processing, i.e. sintering or infiltration. It should be noted that the post processing influences the tissue response.

Concerning porosity, interconnected pores having diameters between 100 and 500 µm are the prerequisite for the vascularization of the implanted scaffold [5]. Consequently, the porosity of the scaffolds is one of the most important criteria for optimization. Their quantification using well-established techniques such as Hg-porosimetry and electron microscopy is problematic and does not yield a satisfying description [6] as previously uncovered for another kind of porous scaffolds for bone augmentation [7]. As the alternative to the classical techniques for porosity measurement, micro computed tomography (µCT) provides the necessary spatial and density resolution to analyze the sizes and morphologies of the open and closed pores.

The aim of this study is to analyze the internal structure of bone grafts fabricated by 3D printing and post processing procedures.

2. MATERIALS AND METHODS

Building Material

Spray-dried hydroxyapatite granules (V12) with a mean particle size of 52 µm were chosen for this study. These granulates contain polymeric additives to improve bonding and flowability that is necessary for 3D printing. The water-soluble polymer blend Schelofix was used as binder. These materials were obtained from the Friedrich-Baur-Institute (Bayreuth, Germany).

Scaffold Design and Fabrication

Rapid prototyping requires 3D datasets for manufacturing physical models. In case of designing a patient specific implant, anatomical information can be obtained by computer tomography (CT). In this study we used simplified test geometries, which were constructed using the software tool MIMICS (Materialise, Belgium). Furthermore, MAGICS was also used for slicing the 3D data into a stack of two-dimensional bitmap files. The printer control software of the 3D printer can only process such bitmap files.

A 3D printing test setup [8] was used for scaffold fabrication. The flexibility of this 3D printing setup makes it possible to investigate both modified process techniques and different material combinations. Here, the 3D printer was used with a spatial resolution of 106 dpi and a slice thickness of 200 µm.

Post Processing

All 3D printed green bodies were freed from unglued granulate using an air blower. In this state the scaffolds are fragile and have to undergo a post processing procedure to obtain reasonably stable scaffolds. Two different post-processing procedures were tested: sintering and infiltration.

For sintering the green bodies were carefully transferred in high temperature furnace and sintered in air at 1250 °C for 3 hours.

A medical grade cyanoacrylate (CA)(DYMAX Medi Cure 222) was used for infiltration. The green body was placed on a PTFE membrane, wetted with CA and dried in air for 1 day.

Imaging

For SEM imaging, polished micro-sections of selected test structures were prepared. The test structures were embedded into epoxy resin, grinded to the desired height and afterwards polished using an automatic polishing machine (Minimet1000, Buehler). The SEM micrographs were analyzed using image analysis software (AnalySIS, Soft Imaging Systems).

Synchrotron-based-computed-micro-tomography

Synchrotron-based-computed-micro-tomography (SRµCT) was performed at the beamline BW 2 at HASYLAB (DESY, Hamburg, Germany) in absorption contrast mode [9] using the photon energy of 24 keV. The voxel length corresponds to 4.3 µm. The spatial resolution was determined using the modulated transfer function of a gold edge to 6.4 µm [10]. 3D data were reconstructed out of 720 projections by the filtered back-projection algorithm [11].

Image analysis

For image analysis the slice images were cropped using the software AnalySIS (Soft imaging Systems, Münster, Germany). Line profiles for binarization were calculated using the same software package. The distance transforms for quantitative 3D porosity characterization were obtained by the means of the Gigatools software [12].
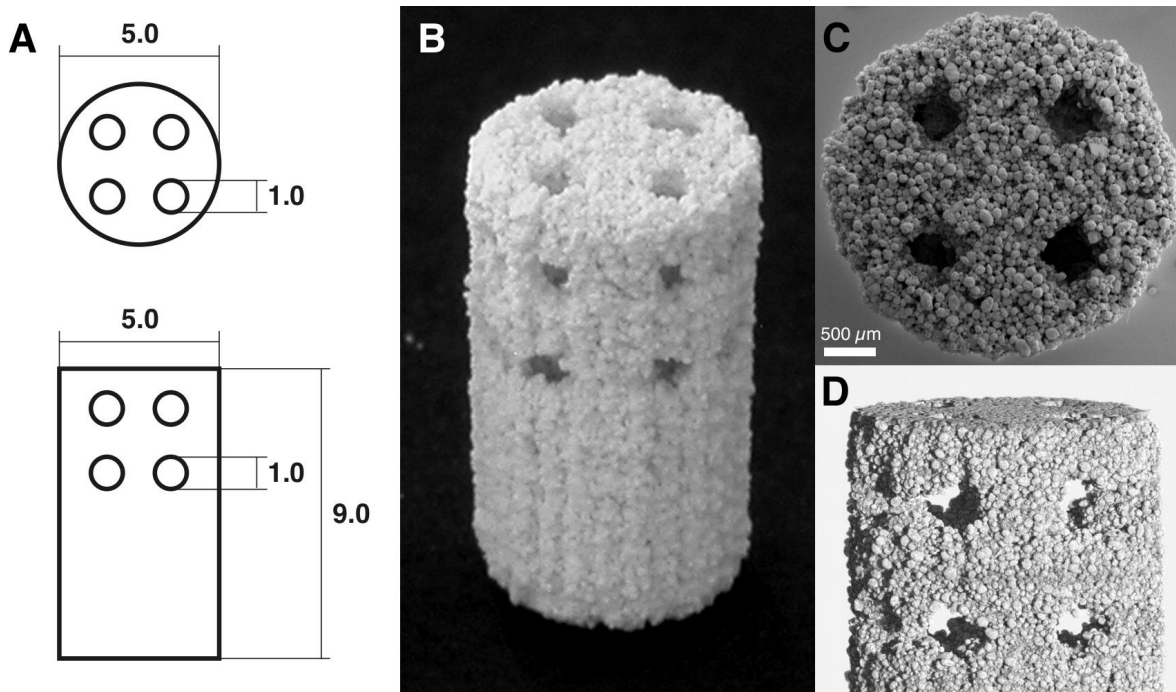

Fig. 3 A: CAD-representation of the test scaffold (measures are in mm). B: Photography after 3D printing and sintering. C: SEM image of the surface (top view) of the scaffold. D: Representation of the SRµCT dataset.

3. RESULTS AND DISCUSSION

Scaffold Design

Using the presented RP technique, it is possible to manufacture scaffolds as shown in figure 1. The outer shape of this structure was adapted to the beam size of beamline BW2 at HASYLAB. To achieve comparable information out of each experiment, the scaffold consists of two parts: the lower half is built solid while the second part possesses an interconnected channel structure. The solid part ought to give information about the micro- and nanoporosity (compare figure 6) of the scaffold and the granules itself. The upper part of the scaffold possesses 8 crossing channels, 4 vertically

aligned and 4 in horizontal alignment. The channel diameter d_c is 1 mm. This is quite large for vascularization of the scaffold. Taking into account a distinct shrinkage of these channels, caused by densification during the sintering process or a partial filling with infiltration liquid, the channel diameters of the post-processed scaffolds are expected in a size range of $d_c \approx 500$ µm. Table 1 gives an overview of the investigated scaffold sizes.

Table 1: Sample description of investigated scaffolds. d_c = diameter of internal channels.

Sample ID	Size (mm)	Post Processing	Threshold[a]
P1	$d = 5$, $h = 9$, $d_c \approx 1000$ µm	Green body	66 (GP), 65 (LP)
P2	$d = 3$, $h = 6$, $d_c \approx 650$ µm	Sintered at 1250 °C	115 (GP), 113 (LP)
P3	$d = 5$, $h = 9$, $d_c =$ n. m.	Infiltrated with DYMAX MediCure 222	n.m.

[a] GF = Gaussian fit, LP = line profiling, n.m. = not measured

Image processing

Figure 4 shows a selected SRµCT slice image of the sample P2. All images were cropped to regions of interest (ROI) suitable for image processing as can be seen in left and middle images. Rectangular regions were selected for image analyses, because the frayed border of the samples allowed no satisfying masking of the samples border. The ROIs were selected to contain a maximum of the sample way and to include all channels of the internal structure.

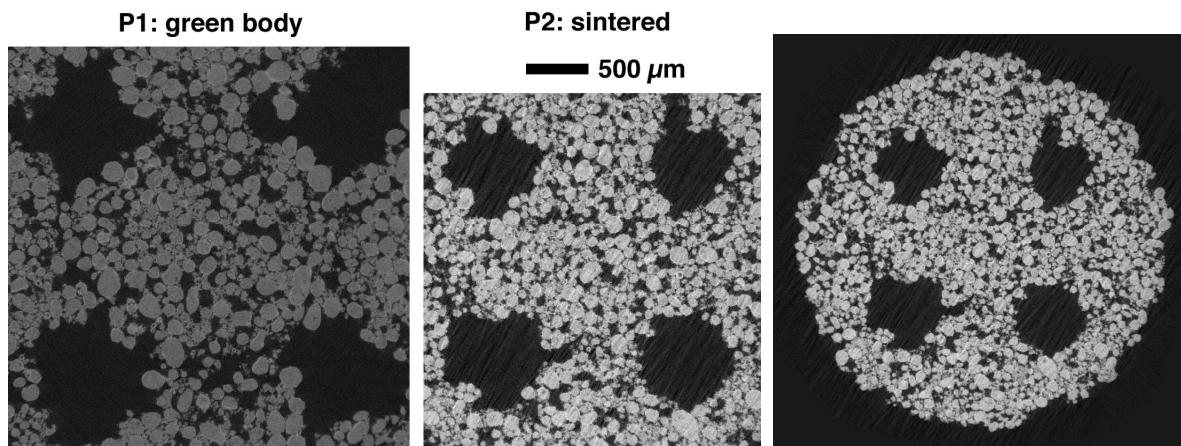**P1: green body**   **P2: sintered**   ▬ **500 µm**

Fig. 4: Slice representation of samples P1 and P2. The left and middle images show the region of interest (ROI) used for image analysis. The right image shows a slice of the complete sample P2. The difference in density between sintered and thermally untreated material can easily be seen.

Thresholding

The SRµCT images, scaled in 256 grey-values, must be converted to binary images discriminating between material and air. In a first attempt, we tried setting the threshold to the crossing point of the two Gaussians, determined from a combined fit of the experimental data. Figure 5 shows the histogram of sample P2, which is a typical example of these ceramic scaffolds. Here the Gaussian fit of the data was impossible due to a relatively high number of voxels exhibiting the absorption between air and hydroxyapatite. This number is by far higher as expected from background noise and partial volume effects. It has its origin in a nanoprosity of the HA-granules below the resolution limit of SRµCT, here 4.3 µm. Figure 5 shows a polished cross section of a 3D printed and sintered scaffold. The nanoporosity of the granules can be easily seen as white domains in the light-grey HA-granules. The detail image of a selected granule in figure 6

shows the enclosed pore even better. Here the pore is filled with the embedding epoxy resin denoting that the pore is open to the outside of the granule.
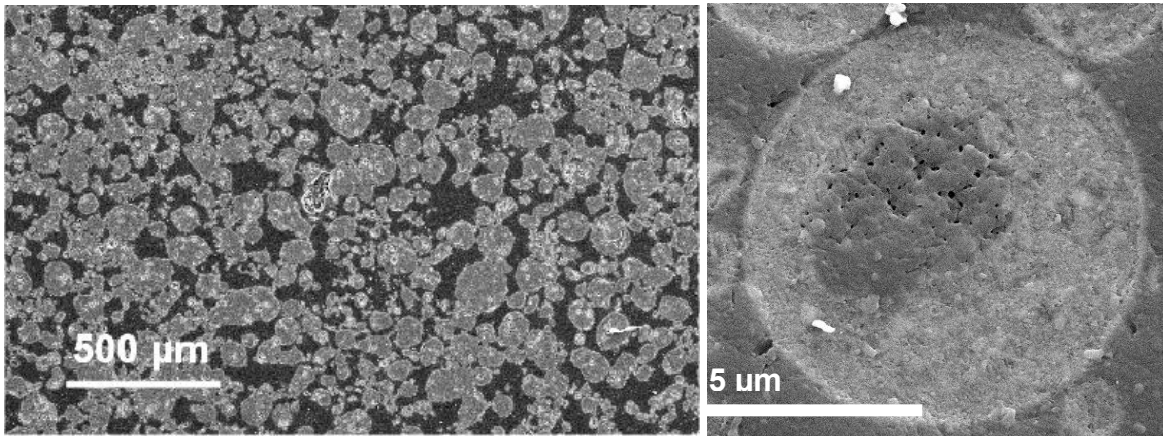

Fig. 5: SEM micrograph of a 3D printed and sintered HA scaffold The dark regions represent the embedding epoxy resin while the lighter gray areas are the ceramic material. The white areas are closed nanoporosity of the HA-granules.

Fig. 6: SEM micrograph of a representative HA granule prior to the 3D printing process. The dark regions represent the embedding epoxy resin while the lighter gray areas are the ceramic material. The white spots are artifacts produced during sample preparation
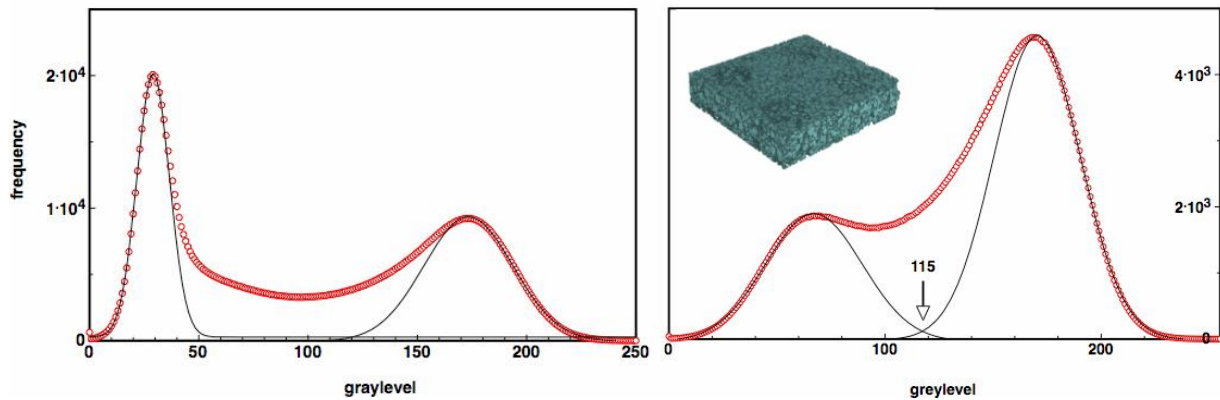

Fig. 7 Histogram of sample P2. Depicted are the summarized data of all slices. The red colored circles represent the measured data and the solid lines are Gaussian fits.

Fig. 8: Histogram of a selected ROI of sample P2. The red colored circles represent the measured values, the solid lines are Gaussian fits. The insert shows 3D representation of the selected ROI.

We tried two different approaches to determine an objective threshold level: using a region of interest and line profiling. Figure 8 shows the resulting histogram of the solid region of interest (P2). Using this reduced dataset, a Gaussian fit of both peaks was possible on the basis of the Levenberg / Marquardt algorithm using the ProFit computer program. We set the threshold level to the crossing point of the two Gaussians at a gray value of 115. Indeed this result was still not satisfying, because of the fact that a combined Gaussian fit still was impossible. In order to approve the result additional line profiling on selected images was performed. Finally, 10 images of each sample (P1 & P2) were selected and a total of 20 line profiles were selected in each case. The line length was set to 50 voxels with respect to the diameter of the selected granules. Figure 9 shows the result of the result of the profile plots while the numerical details are denoted in table 1. The resulting threshold levels are in accordance to the results derived from the Gaussian fits and result to threshold levels of 66 (P1) and 114 (P2).
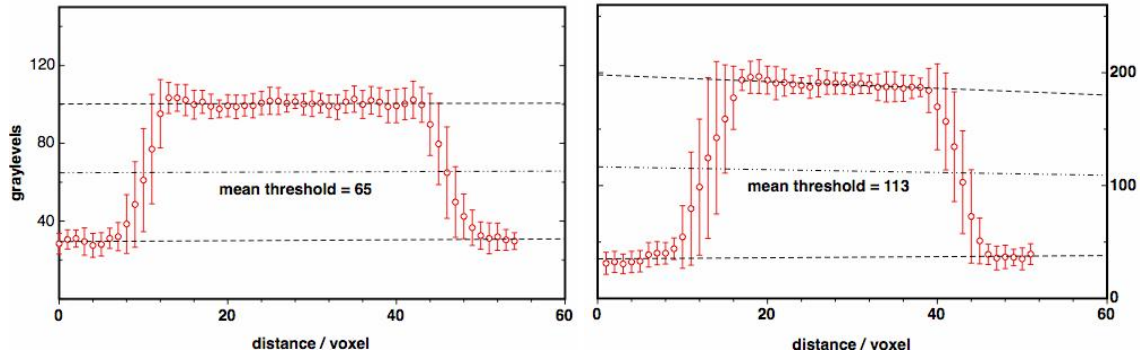
Fig. 9: Line profiling of samples P1 (left) and P2 (right). The red circles represent the mean values of 20 selected granules. The dotted lines are the fits of the upper and lower gray level, which represent air and material.

Post Processing: sintering

The standard post-processing we use for the 3D printed HA scaffolds is sintering at temperatures between 1200 and 1300 °C. Due to the ceramics densification during the firing a shrinkage of about 25% occurs, combined with a significant enhancement of mechanical stability [13]. In order to quantify the effect of sintering on the internal scaffold structure, information about the porosity of the scaffolds is needed. To achieve the mean pore diameter the ratio of volume to surface has to be calculated. Since the extraction of the surface is hardly detectable for complex scaffolds like the ones used for this study, we calculated 3D distance transform, an alternative approach to gather porosity information. In this method the minimal distance of each voxel to material is determined [12]. Figure 10 shows the 3D distance maps of representative slices of P1 and P2. The 25% shrinkage of P2 is obvious. Changes of the internal structure on the other hand are not present.
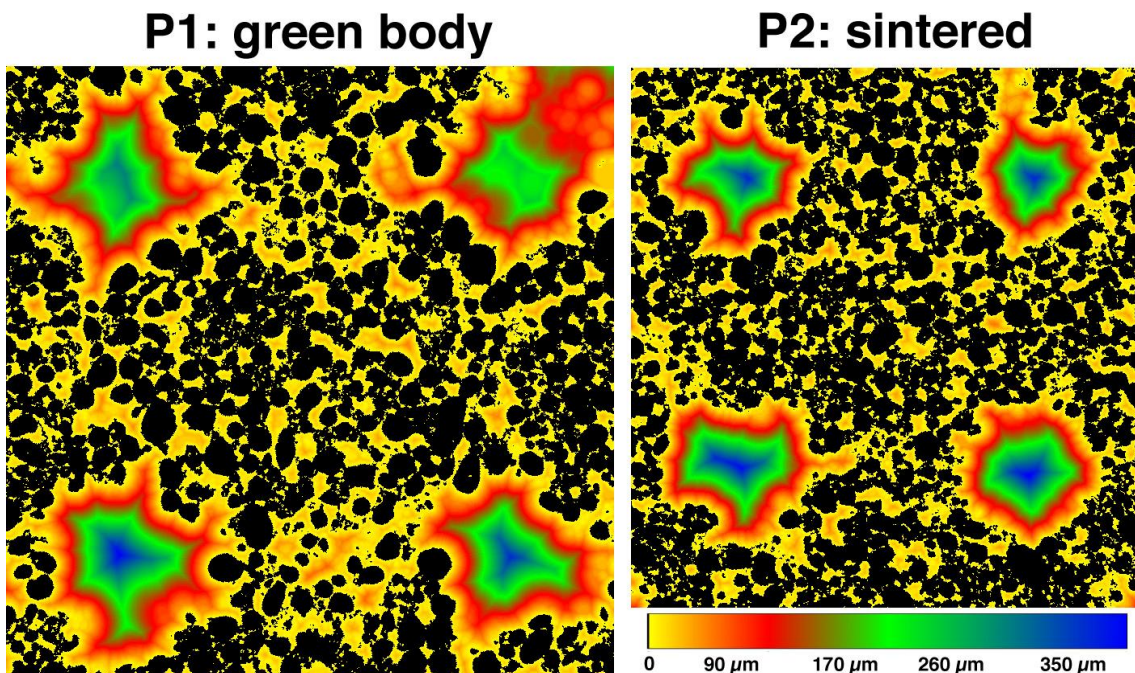

Fig. 10:Distance transform of selected slices of P1 and P2. The slices were selected according to figure 5. Black represents the material itself. The other colors correspond to voxels with the distances to material denoted in the calibration bar.

The distribution function shown in figure 11 demonstrates the effect of sintering on the internal structures. A significant difference between both samples is visible for distances above about 30 voxels (120 µm). The total porosity of both

scaffolds is reduced from 52% (P1) to 49% (P2) during sintering. For the sintered sample these values are in accordance to an earlier porosity determination of 3D printed HA scaffolds using Hg porosity [14]. For the green bodies we were able to calculate a reproducible porosity, for the first time. This kind of samples cannot be analyzed using established methods, due to their fragility.
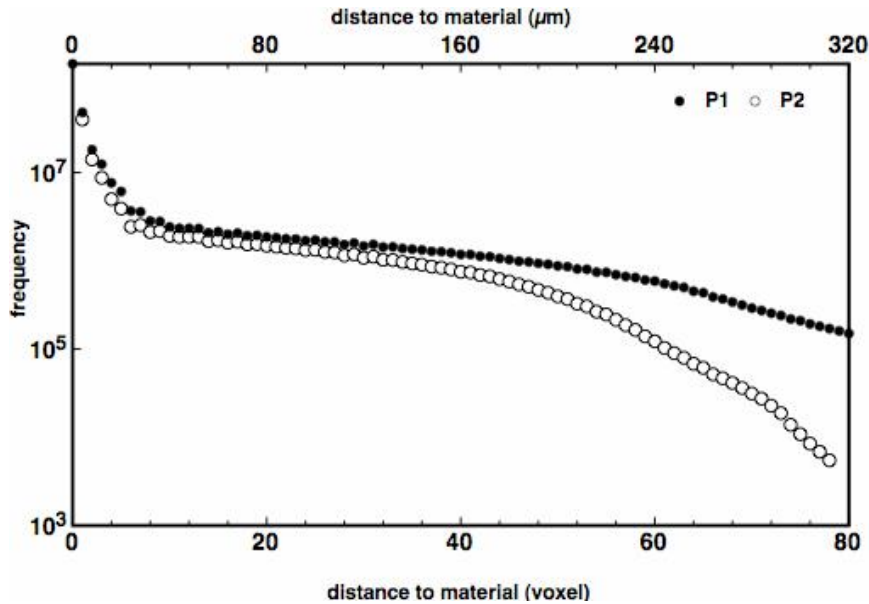

Fig. 11:   Distance distribution for HA-scaffolds P1 and P2

Post Processing: infiltration

The disadvantage in using sintering for post processing is the fact that HA looses its resorbability [15]. To achieve a possibility for the fabrication of resorbable scaffolds providing a sufficient mechanical stability for safe and easy handling, we tested infiltration as alternative post processing procedure. For this preliminary test a medical grade cyanoacrylate was used. The advantage of Cyanoacrylate is that it reacts with the OH-groups of the HA to form a hard composite.

Figure 12 shows the histogram of P3, which was post processed using infiltration. Here the density resolution in the slices is insufficient for a quantitative interpretation. Nevertheless, a qualitative interpretation of the results is possible. The infiltration medium penetrates the sample completely and closes most of the micro-pores as can easily be seen in figure 13. Even more obvious, there is the tendency that the infiltration medium also fills the interconnected channels of the structure. As a result, infiltration is a promising alternative post processing. By changing the infiltration protocol, the clogging of the macrospores should be avoidable. Using resorbable polymers for infiltration this opens great opportunities for the fabricating of an alternative class of composite scaffolds with promising properties for bone replacement.
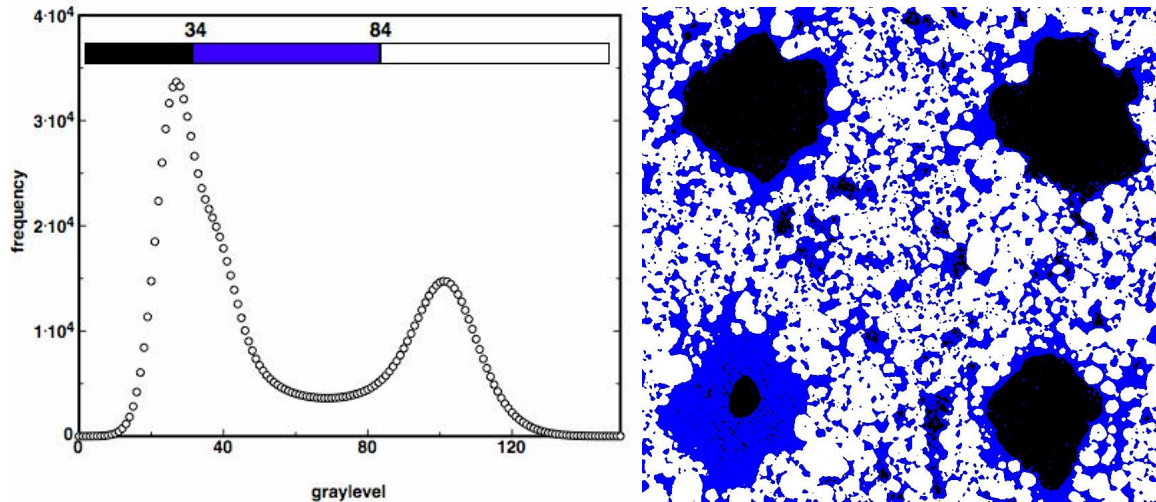
Fig. 12: Histogram (left) of P3, summarized over all slices.

Fig. 13: False color representation (right) of a representative slice of P3. In this image black color represents air, white is material and the infiltration polymer is colored blue.

In conclusion, 3D printing is a promising technology for the fabrication of highly porous scaffolds. Synchrotron – radiation-based-μCT is a powerful tool to quantify the internal microstructure of 3D printed scaffolds.

4. ACKNOWLEDGMENT

REFERENCES

1.   S.M Schnürer,.U. Gopp, K. Kühn, S. J.Breusch, Knochenersatzwerkstoffe, *Orthopädie*, 32, (2003).

2.   T. Wohlers, Wohlers report 2004: Rapid prototyping & tooling state of the industry. Fort Collins, CO: Wohlers Associates, (2004).

3.   S. H. Irsen, H. Seitz,C. Tille, G. Bermes, E. Wolfinger, R. Sader, H.-F. Zeilhofer, Anatomical Rapid Prototyping models with soft and hard tissue representation for surgical planning. ESEM 2003: *Technology and Health Care* Special Issue 12, 110-111, (2004).

4.   S. V. Dorozhkin, M. Epple , Die biologische und medizinische Bedeutung von Calciumphosphaten, *Angew. Chem.* 114, 3260 – 3277, (2002).

5.   O. Gaulthier, J.M. Boouler, E. Aguado, P. Pilet, G. Daculsi, *Biomater*. 19, 133-139 (1998).

6.   B. Bruckschen, H. Seitz, T.M. Buzug, C. Tille, B. Leukers, S. Irsen, *Biomedizinische Technik* 50 Suppl. 1/2, 1609-10 (2005).

7.   F.A. Maspero, K. Ruffieux, B. Müller, E. Wintermantel, J. *Biomed. Mater. Res*. 62, 89-98 (2002).

8.   Seitz, H.; Rieder, W.; Irsen, S.; Leukers, B.; Tille, C.: Three-dimensional printing of porous ceramic scaffolds for bone tissue engineering. *J Biomed Mater Res Part B: Appl Biomater*, 74B, 782–788, (2005).

9.   F. Beckmann, in Developments in X-ray Tomography III, edited by U. Bonse (SPIE - The International Society for Optical Engineering, San Diego, USA, 2001), Vol. 4503, p. 34.

10. B. Müller, P. Thurner, F. Beckmann, T. Weitkamp, C. Rau, R. Bernhardt, E. Karamuk, L. Eckert, S. Buchloh, E. Wintermantel, D. Scharnweber, H. Worch: Three-dimensional evaluation of biocompatible materials by microtomography using synchrotron radiation, Proceedings of SPIE 4503 178-188, (2002).

11. A. C. Kak and M. Slaney, Principles of Computerized Tomographic Imaging (Society of Industrial and Applied Mathematics, 2001).

12. B. Müller, F. Beckmann, M. Huser, F. Maspero, G. Szekely, K. Ruffieux, P. Thurner, E. Winter¬mantel Biomol Engin 19:73-8, (2002).

13. H. Seitz, H.; S. H. Irsen, B. Leukers, W. Rieder, C. Tille, Mechanical properties of porous ceramic scaffolds made by 3D printing. *Advanced Research in Virtual and Rapid Prototyping* 1, 109-113, (2005).

14. B. Bruckschen, H. Seitz, T.M. Buzug, C. Tille, B. Leukers, S. H. Irsen, Comparing Different Porosity Measurement Methods for Characterisation of 3D Printed Bone replacement Scaffolds, *Biomedizinische Technik* 50 Supplementary Vol. 1,2 1609 -10 (2005).

15. D. Tadic, M. Epple, A thorough physicochemical characterisation of 14 calcium phosphate-based bone substitution materials in comparison to natural bone, Biomaterials 25, 987–994 (2004).